JTTEE5 8:219-222




# Vacuum-Plasma Sprayed Nanostructured Titanium Oxide Films

*Y. Zhu, M. Huang, J. Huang, and C. Ding*

*(Submitted 30 March 1998; in revised form 14 September 1998)*

**Nanostructured titanium oxide films were fabricated by vacuum-plasma spraying. The microstructure of the films was characterized with SEM, TEM, and XRD. The chemical state of the titanium oxide of the films was analyzed using XPS. The results indicated that the vacuum-plasma sprayed nanostructured titanium oxide films possessed a corallike structure with small pores and agglomerated grains, which was composed of nanosized particles. The main phases of the films were anatase and rutile, and their relative content was determined by the plasma parameters. Low-valence titanium cations were also found in the films.**

**Keywords** anatase, nanostructured film, rutile, titanium oxide, vacuum-plasma spraying

## 1. Introduction

Nanostructured materials are of great interest in many applications and have been the focus of extensive investigations in recent years (Ref 1-3). Various techniques have been used to prepare nanostructured materials, such as the sol-gel process, the gas-condensation process, direct current (dc) reactive magnetron sputtering, radio frequency (rf) magnetron sputtering, and electrochemical deposition (Ref 4-8). Recently, thermal spraying has been used to prepare nanostructured materials. Karthikeyan et al. developed a thermal spraying technique to produce nanoceramic powders and deposits (Ref 9). Tellkamp et al. sprayed a nanocrystalline Inconel 718 coating using a high velocity oxygen fuel (HVOF) thermal spraying facility (Ref 10). Thermal spraying is a new field for preparing nanostructured materials compared with other methods (Ref 11).

In the present work, nanostructured titanium oxide films were deposited by vacuum-plasma spraying and characterized with scanning electron microscopy (SEM), transmission electron microscopy (TEM), x-ray diffraction (XRD), and x-ray photoelectron spectroscopy (XPS). Titania as a semiconductor material, especially in nanostructured state, has wide application in fields of photocatalysis, photoelectric conversion, and gas-sensing measurement (Ref 12-14), and as-prepared porous nanostructured titanium oxide films should have potential application in these fields.

## 2. Experimental Procedure

### 2.1 Preparation of the Spraying Powders

The spray powders used in this work were quite different from conventional spraying powders. They were synthesized through controlled hydrolysis of titanium butoxide in an ethanol aqueous solution. The process of manufacturing spray powders can be briefly described as follows: hydrolysis of titanium butoxide, direct precipitation followed by ethanol rinsing, and drying at 60 to 70 °C under a pressure of $3 \times 10^4$ Pa for 2 h. The morphology of the powders was spherical or ellipsoidal with a size ranging from 50 to 100 nm in diameter, as shown in Fig. 1. Figure 2 shows the powders in an amorphous phase. The details of the powder preparation are described in Ref 15.

### 2.2 Preparation of Nanostructured Titanium Oxide Film

The A-2000 vacuum-plasma spraying equipment (Sulzer Metco AG, Switzerland) was used to deposit nanostructured titanium oxide films. The powders were fed with a Twin-System 10-V (Plasma-Technik AG, Switzerland). The plasma-spraying process was carried out in an inert gas atmosphere under low-pressure conditions. Table 1 summarizes the experiment conditions. The films were deposited on stainless steel substrates that were polished to a mirror finish.

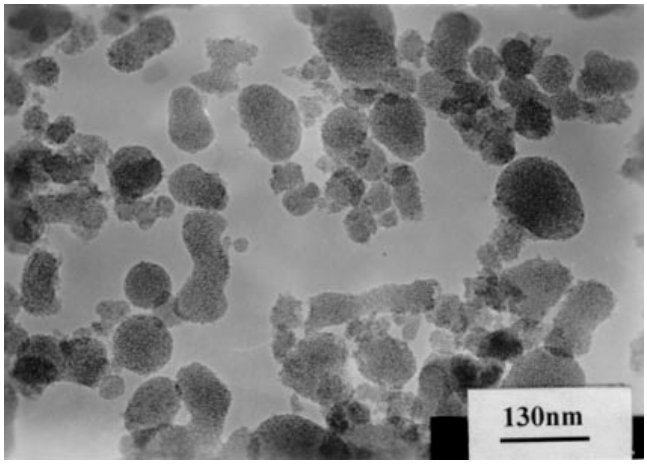


**Fig. 1** TEM micrograph of titanium oxide powders

**Y. Zhu, M. Huang, J. Huang,** and **C. Ding,** Shanghai Institute of Ceramics, Chinese Academy of Sciences, Shanghai, 200050, Peoples Republic of China.

### 2.3 Structural Analysis of Nanostructured Titanium Oxide Film

The thickness of the film was monitored using Talystep equipment (Rank Taylor Hobson, Leicester, UK). The surface morphology of the films was determined with an EPMA-8705QH22 electron probe analyzer (Shimadzu, Tokyo, Japan). The samples were scraped from the substrates and analyzed with a JEM-200CX transmission electron microscope (Jeol, Tokyo, Japan). The crystal structure of the films was measured with a RAX-10 x-ray diffractometer (Rigaku, Tokyo, Japan). X-ray photoelectron spectroscopy analyses were also carried out to examine the chemical state of titanium oxide films with a PHI 5000C ESCE system (Perkin-Elmer, USA).

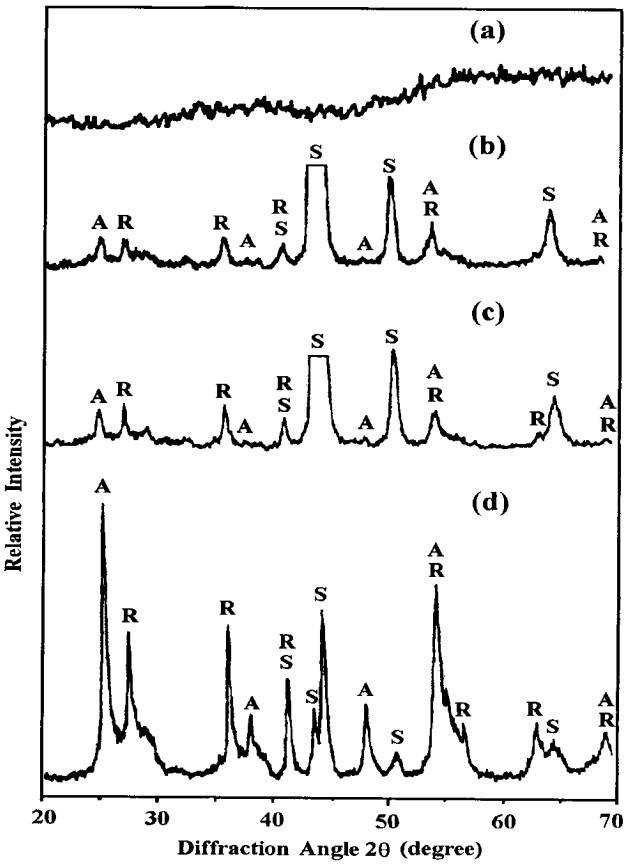


**Fig. 2** XRD patterns of titanium oxide powders and films. (a) Powders. (b) Film (I). (c) Heat-treated film (I). (d) Film (II). A, anatase; R, rutile; S: stainless steel

## 3. Results and Discussion

### 3.1 The Microstructure of the Nanostructured Titanium Oxide Films

Figure 3 presents the TEM micrographs of nanostructured titanium oxide films, which show that both films are composed of irregular-shaped fine grains with particle sizes ranging from 10 to 120 nm. Figure 4 presents the surface morphologies of vacuum-plasma sprayed titanium oxide films, which show that the nanostructured titanium oxide films possess a corallike structure composed of small pores and fine grains.

Vacuum-plasma spraying is a rapid process. The residence time of $TiO_2$ powders inside the plasma jet is less than $10^{-3}$s, therefore, there is little time for $TiO_2$ powders to grow, and the particles in the films remain nanostructured. Plasma-sprayed $TiO_2$ powders slowed and cooled rapidly when they left the plasma jet because of their low mass, so that a porous film rather than a dense film was formed during the plasma-spray process. Nanostructured titania powders were decomposed to some extent in the plasma jet, and this also led to a porous nanostructured film.

**Table 1 Plasma-spraying parameters for nanostructured film (I) and (II)**

| Parameters | Film (I) | Film (II) |
|---|---|---|
| Plasma gas (Ar), flow rate, slpm | 40 | 50 |
| Plasma gas ($H_2$), flow rate, slpm | 6 | 0 |
| Carrier gas (Ar), flow rate, slpm | 2 | 2 |
| Current, A | 500 | 700 |
| Voltage, V | 58 | 33-35 |
| Chamber pressure, mbar | 30 | 30 |
| Distance, mm | 350 | 350 |
| Translation speed, mm/s | 500 | 50 |

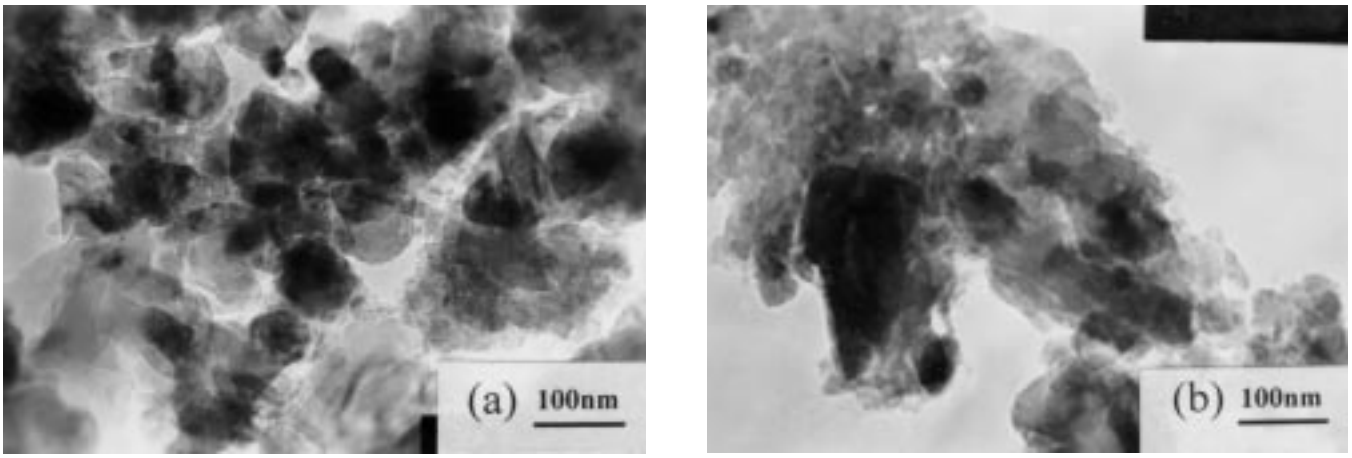


**Fig. 3** TEM micrograph of film (I) and film (II). (a) Film (I). (b) Film (II)

The morphologies of nanostructured titanium oxide films depend on the preparative conditions. At high power and with $H_2$ content in the plasma jet, the morphology of film (I) is relatively smooth and dense and covered with small protuberances, as shown in Fig. 4(a) and (b). However, at low power and without $H_2$ content in the plasma jet, the morphology of film (II) appears rough with fine grains piled up loosely, as shown in Fig. 4(c) and (d). The spraying power and the components of plasma gas should be the main factors influencing the microstructure of the films. The spraying power used for film (I) was 29 kW, which is higher than that used for film (II) (~22 kW). The plasma gas $H_2$ played an important role in the process of plasma spraying. First, the addition of plasma gas $H_2$ elevated the spraying power; second, the plasma gas $H_2$ was beneficial for heat transfer between the plasma jet and powders. Higher power and better heat transfer improved the melting state of powders. Thus, film (I) was smooth and dense relative to film (II).

### 3.2 X-Ray Photoelectron Spectroscopy Analyses

Figure 5 shows XPS spectra of the nanostructured titanium oxide film. The binding energy peaks of Ti(2p) were regressed. The results reveal that there were two different binding states of titanium cations in the titanium oxide film. Peaks at 464.8 and 459.2 eV correspond to the binding energies of the $Ti(2p^{1/2})$ and $Ti(2p^{3/2})$ of $Ti^{4+}$ cations. Peaks at 461.8 and 457.4 eV were the binding energies of the $Ti(2p^{1/2})$ and $Ti(2p^{3/2})$ of low-valence titanium cations. The formation of low-valence titanium cations indicated the deoxidization of $TiO_2$ powders during the plasma-spraying process, and the deoxidization resulted in the formation of oxygen vacancies in the films.

### 3.3 The Crystal Structure of Nanostructured $TiO_2$ Films

Figure 2 shows the x-ray diffraction patterns of the powders and as-sprayed films. It can be seen that the amorphous state of the powders changed into anatase and rutile phases, which indicated that crystalline cores nucleated and grew during the process of plasma spraying. The diffraction intensity of anatase phase was similar to that of the rutile phase in film (I). However, in film (II), the diffraction intensity of anatase phase was slightly higher than that of rutile phase, which indicates that the quantity of anatase phase increased relative to rutile phase in film (II). The XRD pattern of film (I) after heat treating at 250 to 300 °C in atmosphere for 30 min is shown as curve c in Fig. 2. It can be seen that the diffraction intensity of film (I) had no apparent change after heat treatment, however, the interplanar distance of heat-treated film (I) changed slightly compared with that of as-prepared film (I). Table 2 presents the interplanar distances determined in this work and from the Joint Committee on Powder Diffraction Standards (JCPDS) (Ref 16). From this table, it can

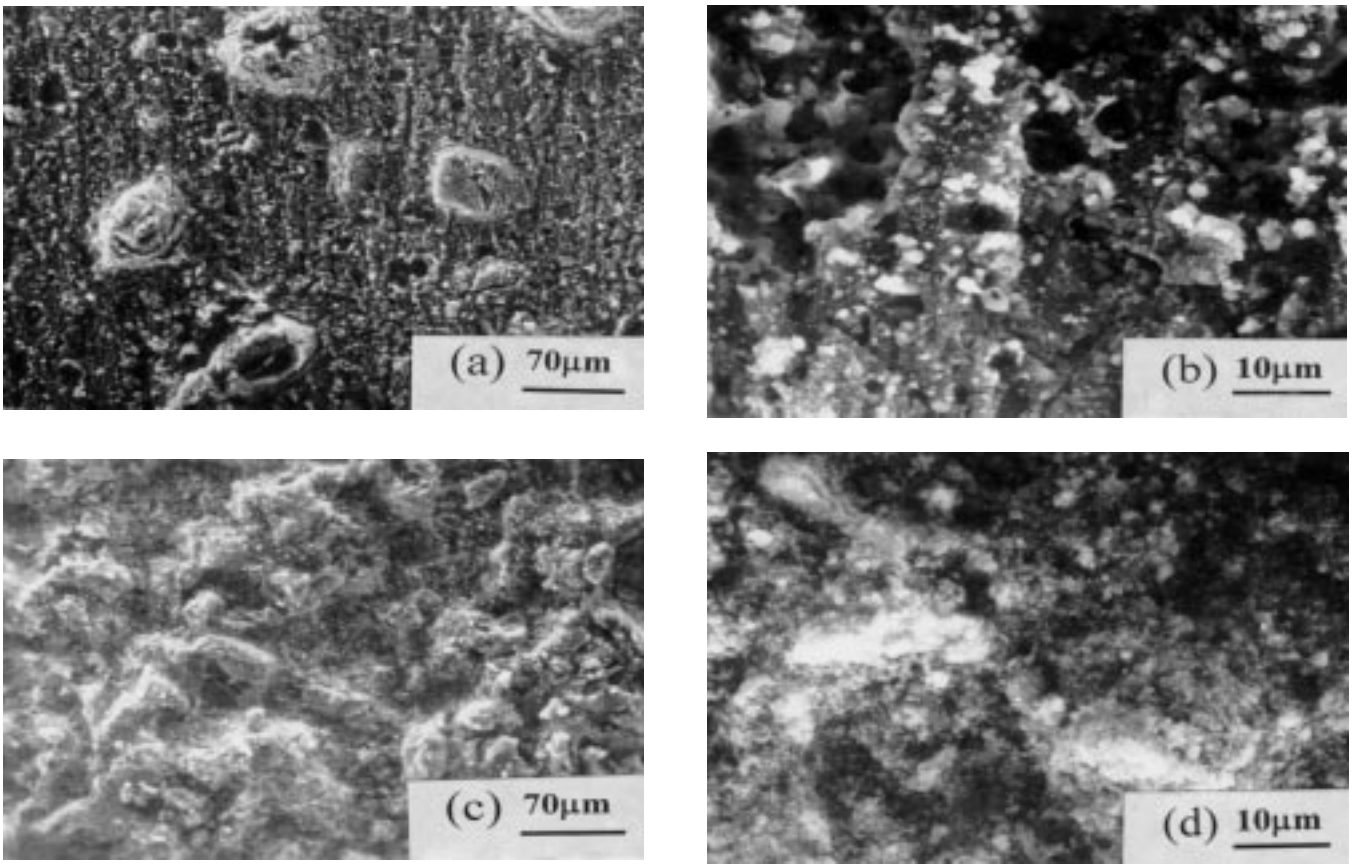


**Fig. 4** SEM micrographs of vacuum-plasma sprayed titanium oxide films. (a) and (b), film (I). (c) and (d), film (II)

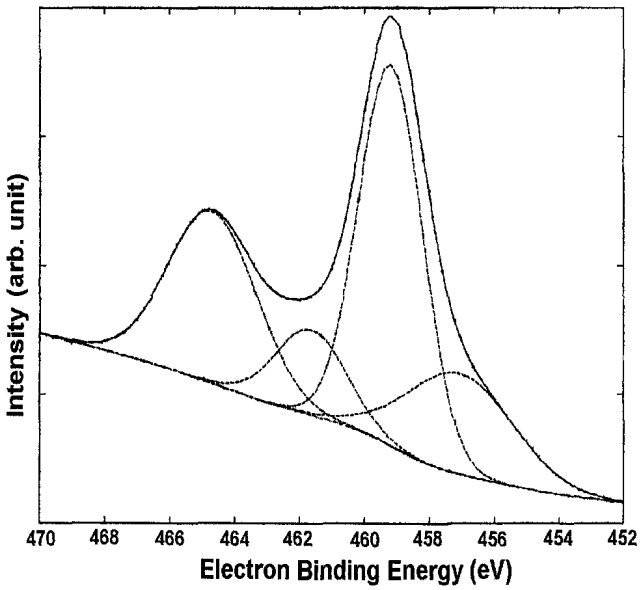


**Fig. 5** XPS spectra of film (I): Ti(2p) peaks

**Table 2 The interplanar distance of anatase and rutile phases in vacuum-plasma sprayed nanostructured films**

| Material | $d_{101}$ of anatase, Å | $d_{110}$ of rutile, Å |
|---|---|---|
| Film (I) | 3.477 | 3.226 |
| Film (II) | 3.490 | 3.225 |
| Heat-treated film (I) | 3.500 | 3.230 |
| From JCPDS | 3.520 | 3.247 |

be seen that both $d_{101}$ of anatase and $d_{110}$ of rutile in film (I) and film (II) are smaller than that of JCPDS, and $d_{101}$ of anatase in film (I) increased after heat treatment in atmosphere.

The high temperature and low pressure of the spray process led to deoxidization of the spray powders, and therefore, resulted in the formation of oxygen vacancies in the film, as shown by XPS analyses. These oxygen vacancies induced a decrease of the interplanar distance. When the film was heat treated in air, oxygen atoms were added to the vacancies of the film, and the interplanar distance of anatase and rutile phases increased.

Comparing curves d and b in Fig. 2, it can be seen that the diffraction intensity of film (II) is higher than that of film (I), because film (II) was thicker than film (I). The surface profilometry analyses showed that the thickness of film (I) was approximately 0.4 μm and that of film (II) was 1.2 μm. The diffraction intensity of the titania film increased and that of stainless steel substrate decreased with increasing the thickness of films.

## 4. Conclusions

In this study, porous nanostructured titanium oxide films were deposited by vacuum-plasma spraying. The $TiO_2$ film possessed a corallike structure with small pores and aggregated grains, which were composed of nanosized particles. The main crystal phase of the films was composed of anatase and rutile. The microstructure of the films and the relative amounts of anatase and rutile were determined by the plasma-spraying parameters. High power and better heat transfer of the plasma jet led to smoother and higher density films, as well as more rutile phase. Low-valence titanium cations were formed during the plasma-spray process.

## References


1. G. Yang, H. Zhuang, and P. Biswas, Characterization and Sinterability of Nanophase Titania Particles Processed in Flame Reactors, *Nanostructured Mater.*, Vol 7 (No. 6), 1996, p 676-689
2. T. Takagahara, Effects of Dielectric Confinement and Electron-Hole Exchange Interaction on Excitonic States in Semiconductor, *Phys. Rev. B, Condens. Matter*, Vol 47 (No. 47), 1993, p 4569-4584
3. A. Hagfeldt, N. Vlachopoulos, and M. Grätzel, Fast Electrochromic Switching with Nanocrystalline Oxide Semiconductor Films, *J. Electrochem. Soc.*, Vol 141 (No. 7), 1994, p L82-L84
4. E. Haro-Poniatowski, R. Rodriguez-Talavera, M. De La Cruz Hevedia, O. Cano-Corona, and R. Anoyo-Murillo, Crystallization of Nanosized Titania Particles Prepared by the Sol-Gel Process, *J. Mater. Res.*, Vol 9, 1994, p 2102-2108
5. J. Lu, J. Wang, and R. Rai, Solution Precursor Chemical Vapor Deposition of Titanium Oxide Thin Films, *Thin Solid Films*, Vol 204, 1991, p L13-L17
6. M.H. Suhail, G.M. Rao, and S. Mohan, Dc Reactive Magnetron Sputtering of Titanium-Structural and Optical Characterization of $TiO_2$ Films, *J. Appl. Phys.*, Vol 71 (No. 3), 1992, p 1421-1427
7. H. Li, W. Luo, X. Chen, A. Ding, and Z. Zhuang, Preparation of Nanocrystalline PLT Thin Films by RF Magnetron Sputtering, *J. Inorg. Mater.*, Vol 9 (No. 3), 1994, p 371-374
8. M. Shirkhanzadeh, Fabrication and Characterization of Alkoxy-Derived Nanophase $TiO_2$ Coatings, *Nanostructured Mater.*, Vol 5 (No. 1), 1995, p 33-40
9. J. Karthikeyan, C.C. Berndt, J. Tikkanen, J.Y. Wang, A.H. King, and H. Herman, Preparation of Nanophase Materials by Thermal Spray Processing of Liquid Precursors, *Nanostructured Mater.*, Vol 9, 1997, p 137-140
10. V.L. Tellkamp, M.L. Lau, A. Fabel, and E.J. Lavernia, Thermal Spraying of Nanocrystalline Inconel 178, *Nanostructured Mater.*, Vol 9, 1997, p 489-492
11. C.C. Berndt and E.J. Lavernia, Thermal Spray Processing of Nanoscale Materials, *J. Therm. Spray Technol.*, Vol 7 (No. 3), 1998, p 411-440
12. V. Sukharev, A. Wold, Y.M. Gao, and K. Dwight, Photoassisted Decomposition of Salicylic Acid on $TiO_2$ and Pd/$TiO_2$ Films, *J. Solid State Chem.*, Vol 119, 1995, p 339-343
13. L.D. Birkefeld, A.M. Azad, and S.A. Akbar, Carbon Monoxide and Hydrogen Detection by Anatase Modification of Titanium Dioxide, *J. Am. Ceram. Soc.*, 1992, p 75, 2964
14. B. O'Regan and M. Grätzel, A Low-Cost, High-Efficiency Solar Cell Based on Dye-Sensitized Colloidal $TiO_2$ Films, *Nature*, Vol 353, 1991, p 737-739
15. J.H. Huang, L. Gao, J.Y. Chen, and D.S. Yan, Controlling Crystallinity of Nano-Titania Powder Prepared by the Hydrolysis of Titanium Alkoxide, *J. Inorg. Mater.*, Vol 11 (No. 1), 1996, p 51-56
16. *Powder Diffraction File*, set 21 to 22, Inorganic Volume, No. PDIS-22IRB, JCPDS International Center for Diffraction Data, 1983